Faceting transitions in crystal growth and heteroepitaxial growth in the anisotropic phase-field crystal model*

Chen Cheng(陈 成)†, Chen Zheng(陈 铮), Zhang Jing(张 静), Yang Tao(杨 涛), and Du Xiu-Juan(杜秀娟)

State Key Laboratory of Solidification Processing, Northwestern Polytechnical University, Xi'an 710072, *China*

(Received 29 November 2011; revised manuscript received 9 July 2012)

We modify the anisotropic phase-field crystal model (APFC), and present a semi-implicit spectral method to numerically solve the dynamic equation of the APFC model. The process results in the acceleration of computations by orders of magnitude relative to the conventional explicit finite-difference scheme, thereby, allowing us to work on a large system and for a long time. The faceting transitions introduced by the increasing anisotropy in crystal growth are then discussed. In particular, we investigate the morphological evolution in heteroepitaxial growth of our model. A new formation mechanism of misfit dislocations caused by vacancy trapping is found. The regular array of misfit dislocations produces a small-angle grain boundary under the right conditions, and it could significantly change the growth orientation of epitaxial layers.

Keywords: phase field crystal, misfit dislocations, heteroepitaxial growth

PACS: 81.15.Aa, 68.55.J−, 02.70.Hm **DOI:** 10.1088/1674-1056/21/11/118103

1. Introduction

The phase-field crystal (PFC) method is a new modeling technique that incorporates the periodic nature of a crystal lattice by considering a free energy functional that is minimized by periodic density fields.[1] The periodic nature of the density field naturally gives rise to elastic effects, multiple crystal orientations, and the nucleation and motion of dislocations.[2] This model bridges the gap between the molecular simulation approaches and the phase-field approach by operating on diffusive-time scales, yet atomic-length scales.[3] Moreover, this model can be related to other continuum field theories such as classical density-functional theory and the atomic density function theory.[4] The PFC method has been successfully used to describe a broad range of phenomena, including multi-grain solidification,[5] soft materials,[6] structural phase transformations,[7] nanocrystalline grain growth,[8] dislocation migration,[9] and epitaxial growth.[10]

With the development in this field, many new variants of the PFC model have been proposed to extend its applicability The PFC model is limited in its ability to model systems with realistic dimensions similar to any model that resolves in the atomic scale.[11] An amplitude expansion of the PFC model was developed to alleviate this limitation by applying a heuristic renormalization group method.[12,13] In addition, Jaatinen *et al.* proposed a new variant of the PFC model known as the eighth-order fit (EOF), to make the model useful for practical applications in materials science. The EOF reproduces certain thermodynamic properties of the given material Fe as closely as possible.[14,15] The original PFC model was developed only for a small set of crystal structures because its singlemode free energy limits the complexity of structural transformations that can be simulated.[16] Therefore, the "two-mode" model has been introduced to provide the additional flexibility in controlling the selection of crystal structures and changing the relative stability of different crystal structures.[17,18]

The anisotropic phase-field crystal model (APFC) was recently put forward by Prieler *et al.* in Ref. [19].

*Project supported by the National Natural Science Foundation of China (Grant Nos. 51075335, 51174168, 10902086, and 51274167) and the NPU Foundation for Fundamental Research, China (Grant Nos. 201109 and NPU-FFR-JC201005).

†Corresponding author. E-mail: 286500935@qq.com

© 2012 Chinese Physical Society and IOP Publishing Ltd

This model can be obtained by replacing the Laplacian with more general differential operators to allow for spatial anisotropy. Simulating anisotropic crystal lattice systems of arbitrary Poisson ratio, as well as condensed matter systems such as colloids and liquid crystals, has a great advantage.[20] In the present paper, we follow the aforementioned direction to modify the APFC model and present a semi-implicit spectral method to numerically solve its dynamic equation of APFC. This procedure results in the acceleration of computations by orders of magnitude relative to the conventional explicit finite-difference scheme that used in Ref. [19].

The rest of the paper is organized as follows. In Section 2, the calculation method and the modified PFC model are given. In Section 3, the faceting introduced by the anisotropy and the morphological evolution in heteroepitaxial growth are discussed. Finally, the conclusions of the study are presented in Section 4.

2. APFC model and the numerical formulation

The APFC model has a dimensionless free-energy functional

$$F = \int \mathrm{d}\, r\Bigg\{\frac{\varphi}{2}\Bigg[\tau + a_{ij}\frac{\partial^2}{\partial x_i \partial x_j} + b_{ijkl}\frac{\partial^4}{\partial x_i \partial x_j \partial x_k \partial x_l}\Bigg]\varphi + \frac{1}{4}\varphi^4\Bigg\}, \quad (1)$$

where φ is the average atomic density, τ represents undercooling, a_{ij} is a symmetric matrix element, and b_{ijkl} is a fourth-rank tensor with the symmetry of an elastic tensor: $i \leftrightarrow j$, $k \leftrightarrow l$, $(i,j) \leftrightarrow (k,l)$. We have attempted to illustrate how the APFC method can be used to examine the morphological instability and dislocations nucleation in heteroepitaxial growth. Modeling this process requires a slight modification of the model to reflect the crystal lattice constant. Thus, according to the derivation of Elder,[21] the dimensionless parameter τ is replaced by the constants q_0 and r, which are related to the crystal lattice constant and undercooling, respectively. In addition, an external potential V is used to model an inert substrate. This external potential is introduced by adding a term coupling V linear to φ in the free-energy functional. This process is given by

$$F = \int \mathrm{d}\, r\Bigg\{\frac{\varphi}{2}\Bigg[r + q_0^4 + q_0^2 a_{ij}\frac{\partial^2}{\partial x_i \partial x_j} + b_{ijkl}\frac{\partial^4}{\partial x_i \partial x_j \partial x_k \partial x_l}\Bigg]\varphi + \varphi V + \frac{1}{4}\varphi^4\Bigg\}, \quad (2)$$

where $q_0 = 2\pi/a_0$, and a_0 is the crystal lattice constant. The form of the external potential is

$$V = V_1[\cos(q_{\mathrm{t}}x)\cos(q_{\mathrm{t}}y/\sqrt{3}) - \cos(2q_{\mathrm{t}}y/\sqrt{3})/2] + \varphi_0, \quad (3)$$

where $q_{\mathrm{t}} = 2\pi/a_{\mathrm{t}}$, and a_{t} is the crystal lattice constant of the substrate, φ_0 is the average value of φ, and V_1 is the strength of the external potential. A perfect hexagonal lattice structure can be obtained for $V_1 = 0.2$. The lattice mismatch, ξ, between the film and the substrate is defined as $\xi = (a_0 - a_{\mathrm{t}})/a_0$. The substrate vicinal angle β can be obtained by transforming the coordinates x and y. The time evolution equation in the dimensionless form is derived as follows:

$$\frac{\partial\varphi}{\partial t} = \Delta\left(\frac{\delta F}{\delta\varphi}\right) = \Delta\Bigg(\frac{\varphi}{2}\Bigg[r + q_0^4 + q_0^2 a_{ij}\frac{\partial^2}{\partial x_i \partial x_j} + b_{ijkl}\frac{\partial^4}{\partial x_i \partial x_j \partial x_k \partial x_l}\Bigg]\varphi + V + \varphi^3\Bigg). \quad (4)$$

The semi-implicit Fourier spectral method can be used to solve the dynamic equation, with a rational assumption of $a_{11}/2 = a_{22}/2 = b_{1111} = b_{2222} = b_{1122}$. We apply differential splitting prior to the discretization. Finally, the numerical discretization of Eq. (4) is written as

$$\frac{\varphi_{k,t+\Delta t} - \varphi_{k,t}}{\Delta t} = -k^2\Bigg\{\Bigg[r + \frac{1}{2}a_{11}(q_0^2 - k^2)^2\Bigg]\varphi_{k,t+\Delta t} + \boldsymbol{A}\varphi + (\varphi^3)_{k,t} + V_k\Bigg\}, \quad (5)$$

where $\boldsymbol{A}$ has the following form:

$$\boldsymbol{A} = q_0 a_{ij}\boldsymbol{k}_i\boldsymbol{k}_j + b_{ijkl}\boldsymbol{k}_i\boldsymbol{k}_j\boldsymbol{k}_k\boldsymbol{k}_l, \quad (i \neq j, k \neq l), \quad (6)$$

where $\varphi_{k,t}$, $(\varphi^3)_{k,t}$, and V_k correspond to the Fourier transform of $\varphi_{k,t}$, φ^3, and V, respectively, and $\boldsymbol{k}$ is the unit vector in the Fourier space. The simulation is conducted on a periodic system of size $1024\Delta x \times 1024\Delta x$ and $512\Delta x \times 1024\Delta x$. The time step ($\Delta t$) is 0.3. Note that the grid size (Δx) must be adjusted according to the value of ξ to ensure the continuity and integrity of the substrate. The stability of time stepping for Eq. (5) is a more complicated issue. In practice, it is found that $\Delta t = 0.3$ is

sufficient for the long-time simulation with large systems. Other constant parameters are chosen as follows: $a_{11}/2 = a_{22}/2 = b_{1111} = b_{2222} = b_{1122} = 1$, $b_{1212} = 0$, $(r, \varphi_0, \xi, \beta)$=$(-0.635, -0.47, 0.06, 6.18^\circ)$.

3. Results and discussion

3.1. Faceting transitions introduced by the anisotropy in two-dimensional crystal growth

The faceting introduced by the anisotropy in two-dimensional (2D) crystal growth is studied in this section. The effect of undercooling is also discussed. Similar to the method used by Choudhary, the anisotropic factor ε is introduced to quantify the anisotropy of the material at the atomic scale. This process is given by $\varepsilon = a_{12}/b_{1111}$. The calculated results with different ε are shown in Fig. 1. The results are obtained by placing a small crystalline cluster with 13 density peaks into the simulation box and allowing the cluster to grow until equilibrium is established. A perfect hexagonal lattice structure can be observed in the case of $\varepsilon = 0$. The increasing anisotropic factor ε leads to a series of faceting transitions which include hexagon, rhombus and the stripe for the shape of the crystal. We have determined a dimensionless parameter σ in order to characterize the structural features. This parameter is defined as the average ratio of the length of adjacent sides of the crystal. The relationships between σ and the anisotropic factor ε are described in Fig. 2.

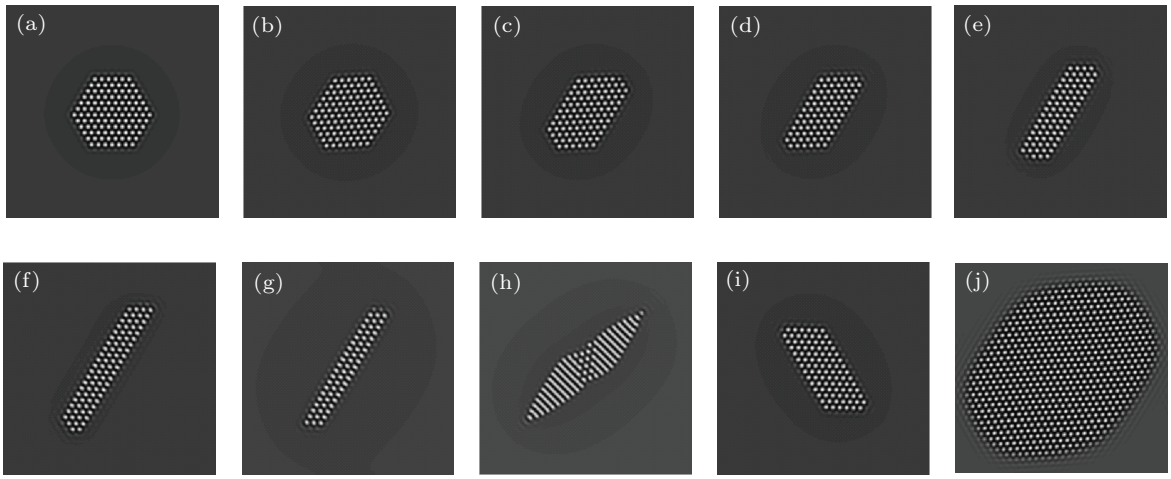


Fig. 1. Faceting transitions which include hexagon, rhombus and the stripe for the shape of the crystal. (a)–(j) correspond to $\varepsilon = 0$, $\varepsilon = 0.5$, $\varepsilon = 0.556$, $\varepsilon = 0.625$, $\varepsilon = 0.714$, $\varepsilon = 0.774$, $\varepsilon = 0.782$, $\varepsilon = 1$, and $\varepsilon = -0.625$, respectively. (j) demonstrates a nonfaceted interface for a high undercooling value of $r = 0.88$.

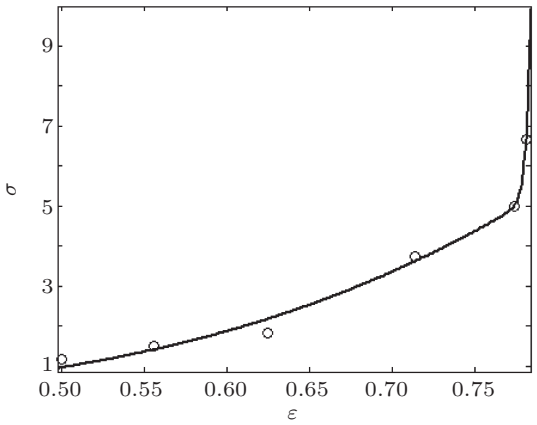


Fig. 2. The relationship between the average ratio σ of the length of adjacent sides of the crystal and the anisotropic factor ε.

These simulation results demonstrate that the stable faceting is only found in the case of $0.5 < \varepsilon < 0.782$. For other positive values of ε, the emergence of the stripe phase will destroy the symmetry of the crystal. Note that the symmetry of the crystal growth can be controlled by the sign of the value of ε. For example, figures 2(d) and 2(i) correspond to $\varepsilon = 0.625$ and $\varepsilon = -0.625$, respectively, at the same time $t = 5000$.

In addition, a high undercooling value of $r = 0.88$ results in the disappearance of faceting and in the reduction of the growth anisotropy (see Fig. 2(j)). This change is mainly caused by the competitive growth among the adjacent sides of the crystal at a high growth rate.

3.2. Morphological evolution in heteroepitaxial growth

In this section, the APFC model is employed to study the coarsening and coalescence of strained islands and the subsequent formation of misfit dislocations on vicinal substrates. The island structures have become an interesting topic in the fabrication of quantum dots or nanowires in lithography-free nanoscale devices.[22,23] Eight layers of substrate atoms reside at the bottom of the simulation cell in the initial conditions. A constant flux boundary condition is maintained along the top boundary, $100\Delta x$ above the film surface, to simulate a finite deposition rate. Numerical simulations are conducted with different ε to illustrate the impact of the anisotropic factor on epitaxial growth.

The calculated results for $\varepsilon = 0.5$ are shown in Fig. 3. The morphological instability of the epitaxial layers is discussed in the framework of the continuum elasticity theory. The elastic strain energy resulting from the lattice mismatch is released in the form of surface energy during the initial stage of film growth. The surface profiles of epitaxial films are dislocation-free islands. The islands tend to grow in fairly uniformly spaced arrays.[24] As the strain islands grow up, the increasing surface energy cannot be compensated by the decrease in the strain energy caused by the lattice mismatch. Thus, the growths of strain islands are restricted. In these conditions, capillarity-driven coarsening, or the competitive growth process wherein some islands grow at the expense of others to minimize the total surface energy, arises.[25] The capillarity-driven coarsening causes the mean island volume to increase with time, during which the number of islands per unit area simultaneously decreases. Finally, film nucleate dislocations are observed on the edge of the islands with the most stress. Islands are no longer coherently strained. The evolution of strain, morphology and interfacial structures are in agreement with the study of Satapathy.[26]

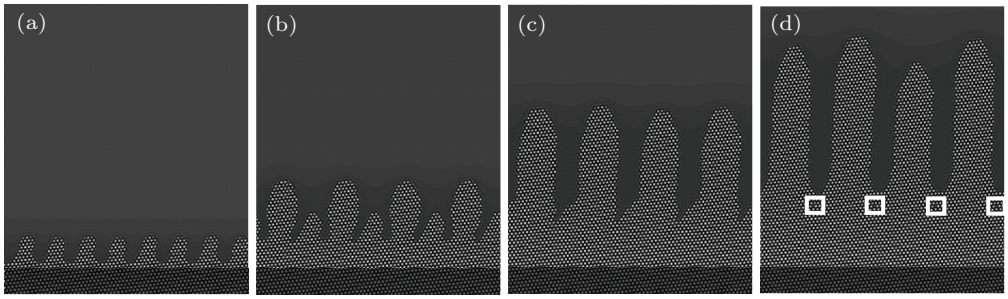


Fig. 3. Coalescence of strained islands and the formation of misfit dislocations on vicinal substrates with $\varepsilon = 0.5$. (a)–(d) correspond to $t = 2400$, $t = 12000$, $t = 28000$, and $t = 50000$, respectively. Dislocations are enclosed by white squares. The substrate is highlighted by a darker gray background. The dislocations are enclosed by white squares.

Figure 4 gives the simulation results for $\varepsilon = 0.532$, and there are several significant changes compared with Fig. 3. From the analysis in Section 3.1, the larger ε indicates an increased ratio σ of the length of adjacent sides. The strained islands undergo a shape transition from hexagon to rhombus. The increase of σ also leads to the growth of strained islands with a tilt angle θ toward the substrate. Figure 5 shows the changes in the tilt angle θ with different ε. An approximate linear relationship is obtained between the two values. With the coarsening and coalescing of the strained islands, the characteristics of oriented growth results in vacancy trapping into the islands (see Fig. 4(c)). This event is analogous to the phenomenon of solute trapping in rapidly solidified alloys.[27] The areas of vacancy trapping can provide sources of stress-relieving dislocations as the coalescing islands continue to grow. This process is different from the traditional formation mechanism of misfit dislocation.[28–30] In addition, figure 4(d) shows that the creation of misfit dislocations changes the growth orientation of coalescing areas. This change in growth orientation will gradually decrease as the dislocations go down to the film–substrate interface.

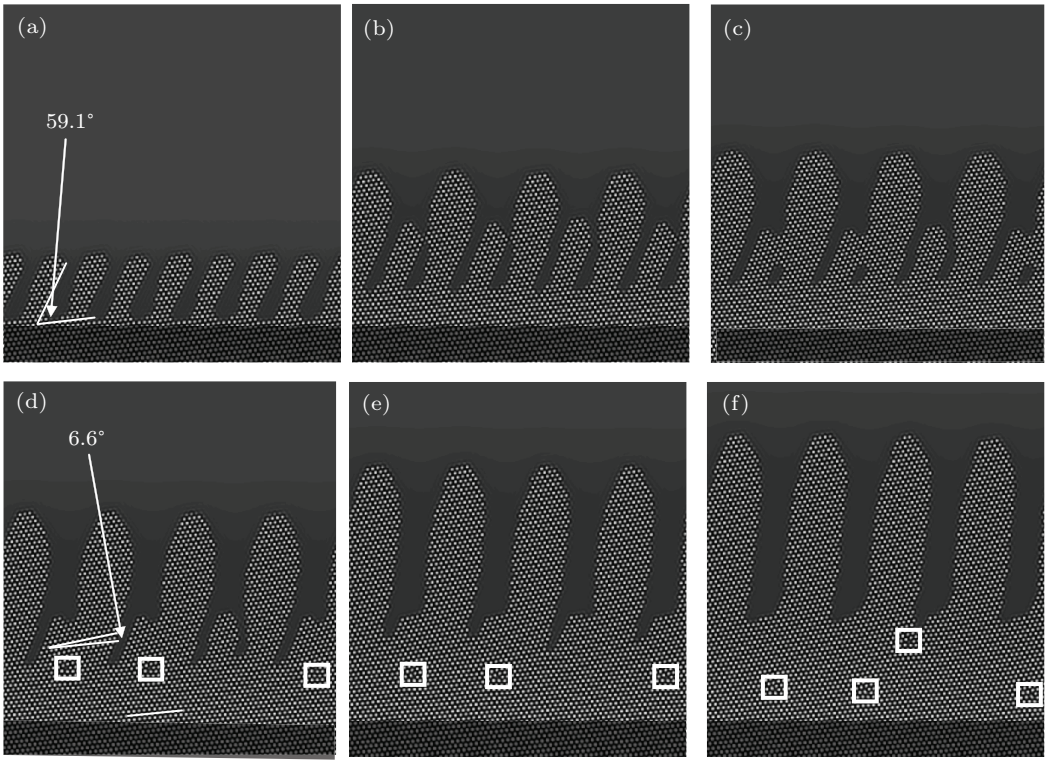


Fig. 4. Shape transition of the strain islands and the creation of misfit dislocations caused by the vacancy trapping for $\varepsilon = 0.532$. (a)–(f) correspond to $t = 2500$, $t = 12500$, $t = 17500$, $t = 22000$, $t = 30000$, and $t = 36500$, respectively. The substrate is highlighted by a darker gray background. The dislocations are enclosed by white squares.

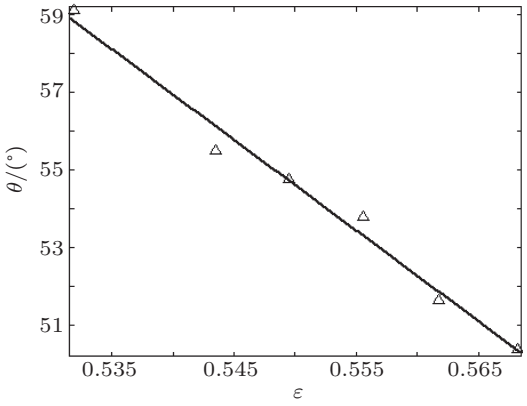


Fig. 5. Relationships between the tilt angle θ and the anisotropic factor ε.

The calculated results for $\varepsilon = 0.568$ are shown in Fig. 6 to further analyze the mechanism of dislocation nucleation caused by vacancy trapping. Compared with Fig. 4, a large number of vacancies are trapped into the films after the coalescence of strained islands, and the film surface begins to approach a planar morphology. We believe that this behavior results from the strain energy concentration at the areas of vacancy trapping. The local free-energy density is depicted in Figs. 6(b) and 6(d) to characterize this phenomenon more clearly. The gray scale is inversely proportional to the local free-energy density. The local free-energy density of the areas of vacancy trapping is clearly higher than the other parts, as shown in the figure. The vacancies gradually disappear with the diffusion of atoms. A periodic array of misfit dislocations eventually appears in the region where the vacancies existed. The regular array of dislocations creates a small-angle grain boundary, as shown in Fig. 6(f). This phenomenon significantly changes the growth orientation of epitaxial layers. The so-called grain-boundary disclinations (rotational defects) are generated in nanocrystalline and polycrystalline films.[31]

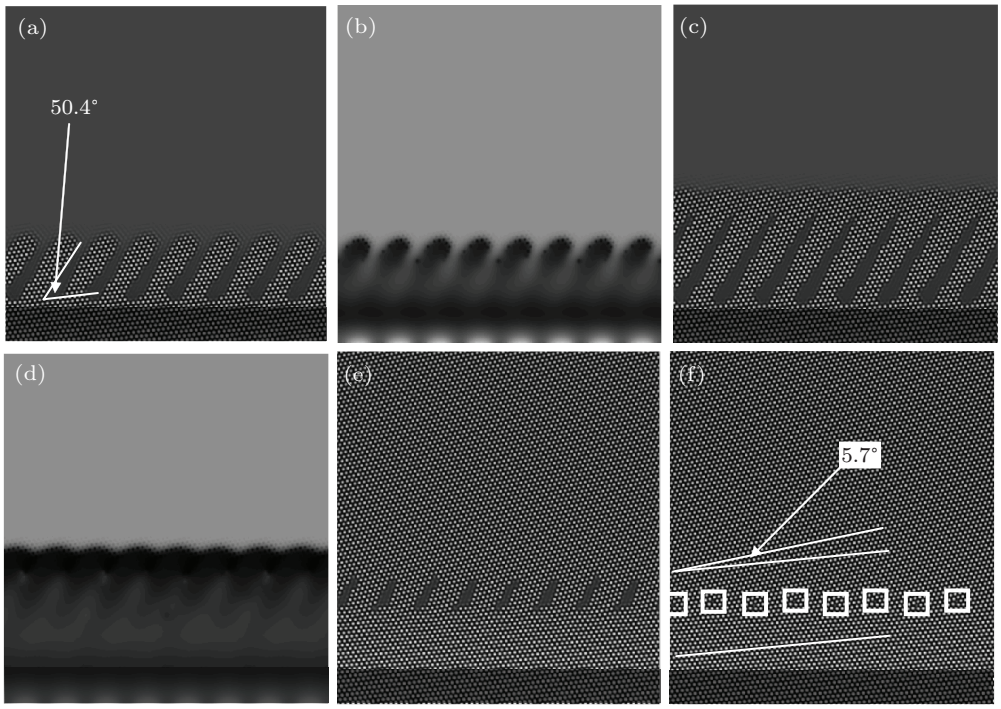


Fig. 6. Vacancy trapping and the formation of a small-angle grain boundary in heteroepitaxial growth. (a)–(f) correspond to $t = 1000$, $t = 1500$, $t = 35000$, and $t = 50000$, respectively. (f) clearly shows a small-angle grain boundary. (b) and (d) correspond to the local free-energy density of (a) and (c). The substrate is highlighted by a darker gray background, and the dislocations are enclosed by white squares.

4. Conclusion

We have modified the APFC model and presented a semi-implicit spectral method to numerically solve the dynamic equation of the APFC model. The faceting transitions introduced by the anisotropy in crystal growth have also been discussed. In particular, we investigated the morphological evolution in the heteroepitaxial growth of our model. The following conclusions were obtained:

i) The application of the new numerical formulation results in the acceleration of computations by orders of magnitude relative to the conventional explicit finite difference scheme. Thus, the formulation allows us to work on a large system and for a long time.

ii) The increasing anisotropic factor ε leads to a series of faceting transitions including a hexagon, rhombus and a stripe for the shape of the crystal. The stable faceting only exists in the case of $0.5 < \varepsilon < 0.782$. For other values of ε, the emergence of the stripe phase will destroy the symmetry of the crystal. The symmetry of the crystal growth can be controlled by the sign of the value of ε.

iii) In heteroepitaxy, it is found that the increasing ε leads to the growth of strained islands with a crystal orientation of several degrees toward to the substrate. The characteristics of oriented growth results in vacancy trapping in the islands with the coarsening and coalescing of strained islands. The areas of vacancy trapping can provide sources of stress-relieving dislocations as coalescing islands grow further. The creation of misfit dislocations can change the growth orientation of coalescing areas. A periodic array of misfit dislocations appears in the region where vacancies existed with respect to a larger ε. The regular array of dislocations makes up a small-angle grain boundary that significantly changes the growth orientation of epitaxial layers.

References

[1] Provatas N, Dantzig J A, Athreya B , Chan P, Stefanovic P, Goldenfeld N and Elder K R 2007 *JOM* **59** 83
[2] Elder K R, Provatas N, Berry J, Stefanovic P and Grant M 2007 *Phys. Rev.* B **75** 064107
[3] Emmerich H, Granasy L and Lowen H 2011 *Eur. Phys. J. Plus* **126** 102
[4] Elder K R, Huang Z F and Provatas N 2010 *Phys. Rev.* E **81** 165421

[5] Zhang Q, Wang J C, Zhang Y C and Yang G C 2011 *Acta Phys. Sin.* **60** 088104 (in Chinese)
[6] Tegze G, Granasy L, Toth G I, Douglas J F and Pusztai T 2011 *Soft Mat.* **7** 1789
[7] Greenwood M, Provatas N and Rottler J 2010 *Phys. Rev. Lett.* **105** 045702
[8] Wu K A and Voorhees P W 2012 *Acta Mater.* **60** 407
[9] Ren X, Wang J C, Yang Y J and Yang G C 2010 *Acta Phys. Sin.* **59** 3595 (in Chinese)
[10] Chen C, Chen Z, Zhang J and Yang T 2012 *Acta Phys. Sin.* **61** 108103 (in Chinese)
[11] Athreya P, Goldenfeld N, Dantzig J A, Greenwood M and Provatas N 2007 *Phys. Rev.* E **76** 056706
[12] Athreya P, Goldenfeld N and Dantzig J A 2006 *Phys. Rev.* E **74** 011601
[13] Elder K R, Huang Z F and Provatas N 2010 *Phys. Rev.* E **81** 011602
[14] Jaatinen A and AlaNissilal T 2010 *Phys. Rev.* E **82** 061602
[15] Jaatinen A, Achim C V, Elder K R and AlaNissilal T 2009 *Phys. Rev.* E **80** 031602
[16] Greenwood M, Provatas N and Rottler J 2011 *Phys. Rev. Lett.* **105** 045702
[17] Wu K A, Adland A and Karma A 2010 *Phys. Rev.* E **81** 061601
[18] Toth G I, Pusztai T, Tegze G, Toth G and Granasy L 2011 *Phys. Rev. Lett.* **107** 175702
[19] Prieler R, Hubert J, Li D, Verleye B, Haberkern R and Emmerich H 2009 *J. Phys.: Condens. Mat.* **21** 464110
[20] Choudhary M A, Li D, Emmerich H and Lowen H 2011 *J. Phys.: Condens. Mat.* **23** 265005
[21] Elder K R and Grant M 2004 *Phys. Rev.* E **70** 051605
[22] Li L B, Chen Z M, Lin T, Pu H B, Li Q M and Li J 2007 *Chin. Phys.* **16** 3470
[23] Liu Y M, Yu Z Y and Ren X M 2009 *Chin. Phys.* B **18** 0016
[24] Wang J P, Zhou W M, Wang C Y and Yin S Y 2008 *Chin. Phys.* B **17** 3008
[25] Floro J A, Sinclair M B, Chason E, Freund L B, Twesten R D, Hwang R Q and Lucadamo G A 2000 *Phys. Rev. Lett.* **84** 701
[26] Satapathy D K, Kaganer V M, Jenichen B, Braun W, Daweritz L and Ploog K H 2005 *Phys. Rev.* B **72** 155303
[27] Tegze G, Toth G I and Granasy L 2011 *Phys. Rev. Lett.* **106** 195502
[28] Albrecht M, Christiansen S, Michler J, Dorsch W and Strunk H P 1995 *Appl. Phys. Lett.* **67** 1232
[29] Teichert C 2002 *Phys. Rep.* **365** 335
[30] Aminpour M, Trushin O and Rahman T S 2011 *Phys. Rev.* B **84** 035455
[31] Ovidko L 2000 *Rev. Adv. Mater. Sci.* **1** 61